RSC Advances

ROYAL SOCIETY OF CHEMISTRY

www.rsc.org/advances

Deployment architecture for controlled morphologies in sessile, mixed colloidal droplets

Prasenjit Kabi[1], Saptarshi Basu[2, 1*], Swetaprovo Chaudhuri[3, 1]

[1]Interdisciplinary Centre for Energy Research,
Indian Institute of Science, Bangalore-560012, India.
[2]Department of Mechanical Engineering,
Indian Institute of Science, Bangalore-560012, India.
[3]Department of Aerospace Engineering
Indian Institute of Science, Bangalore-560012, India.

Colloidal systems offer an effective medium to micro-engineer complex structures without involving sophisticated fabrication procedures. This article presents deployment strategy of multiple droplets of different colloidal composition and utilizes the inherent capillary flow driven self assembly of nanoparticles to construct stacks of multiple materials on a given glass substrate. Here we used aqueous nano-crystalline titania and nano-amorphous silica solutions as the two materials. Initially, pure nanotitania (nanosilica) droplet is deployed and allowed to dry partially. Subsequently, a second droplet of pure nanosilica (nanotitania) is deployed co-axially on the partially dried precipitate. The proposed deployment strategy allowed significant morphological differences when the deployment order of nanosilica and nanotitania were interchanged. Compositional analysis performed using EDX (Energy Dispersive X-ray spectroscopy) showed preferential deposition of nanosilica and nanotitania along the radial as well as the axial plane of the final deposit pattern. The underlying mechanism for such a phenomenon could be attributed to the contact line dynamics of a sessile double droplet. We also observe heteroaggregation of nanosilica-nanotitania interaction along a narrow interface which resulted in nanotitania particles clustering into isolated islands embedded into a matrix of nanosilica particles. Overall, this work elucidates the evaporation driven dynamics of a mixed colloidal system which displays both macroscopic as well as microscopic phenomenon. Such a system could be used to generate ordered arrays of functional materials with engineered micro to nano-scale properties.

*Corresponding author: Tel: +91 080 2293 3367
Email: sbasu@mecheng.iisc.ernet.in (S. Basu)

Introduction

One of the tested methods in semi-conductor manufacturing is chemical vapour deposition which involves mixing materials and subjecting them to heat so that the vapour from the mixture gets deposited on the desired substrate. However, the process requires rather expensive instrumentation. Thus efforts have been made to utilize self assembly of colloidal particles to form naturally occurring structures of myriad complexities [1]. Self-assembly of nanoparticles in a colloidal system can prove to be a very inexpensive and effective method for creating complex array of structures with desired optical, magnetic, electrical and mechanical functionalities [2]. Self-assemblies are achieved under the influence of external force fields such as gravity [3, 4], electrophoresis [5, 6], evaporation induced deposition [7-9], dip coating [10], substrate oscillation [11], fluidic cell technology [12] and sol-gel method [13]. Evaporation driven self-assemblies of sessile droplets provide the simplest of all fabrication strategies [14]. Seminal works on dynamics of sessile droplet evaporation could be found in [15-16]. In nano-colloidal droplets, particles assemble at the pinned periphery due to a radially outward evaporative solvent flux [16-17]. For droplets on hydrophilic surfaces with contact angle of less than 90°, the contact line remains pinned in the initial stages leading to edge deposition of particles to form a ring like structure. Application for such a phenomenon has found its way into various fields. DNA chip manufacturing utilizes natural evaporation of DNA infused droplets to create patterns on glass slides that can be utilized for genotyping and gene profiling [18]. Similarly, chemically patterned substrates are used to obtain precisely shaped and sized crystal structures [19]. Lithography [1], inkjet printing [20] or biomechanical probes for cellular characterization [21] offer few salient examples of applications using droplet evaporation. Tarasevich et al. [22] have experimentally shown the different drying patterns in biological fluids. Guo et al [23] have shown how droplet microfluidics maybe used to obtain high throughput bio-assays. Kang et al [24] have come up with a path breaking technique for bacteria detection in millilitres of diluted blood. However bulk of the work has been done on single, sessile droplets and to our knowledge, no studies exist on the idea of droplet stacking except the one recently reported from our group [25]. The idea is to build a vertical stack of given material(s) of desired morphologies using evaporation induced self assembly over a predefined region on a given substrate. Additive manufacturing relies on the principle of stacking powdered

materials. However, simply stacking one drop over another would lead to spillage and spreading in absence of any external barrier to contain the liquid. In such a scenario, we proposed the double droplet methodology of material stacking that uses capillary flow within the first deployed sessile particle laden droplet to form an initial solid dam like structure [26]. This inner edge of this solid structure (Fig. 1; referred to as agglomeration front (A_f)) has demonstrated the ability to contain liquid from subsequent droplet additions without spillage [25]. It was also demonstrated that by choosing an appropriate time delay between the deployments of two droplets, morphological features of the final deposit pattern could be altered precisely. However, the proof of concept was limited to a single type of nanoparticle. The present paper is tailored to explore the more practically relevant phenomena of multi-component material stacking in thin layers. To this end, double droplet experiments as reported previously [25] were repeated with two droplets, both of same volume and particle concentration differing only in the nature of loaded particles: in the current study we used nanosilica and nanotitania. Strikingly different morphologies of the final deposit pattern were obtained just by the simple act of reversing the order in which nanosilica and nanotitania were dispensed. EDXA (Electron Dispersive Analytical X-ray) of the preserved dehydrated sample revealed preferential segregation (concentration variation) of nanosilica and nanotitania not only along the top layer (spatial extent of ~ 3000 µm) but also across the thickness (~ 25 µm at the edge and ~1 µm at centre of the deposit) of the precipitate. While capillary flow induced particle transport is responsible for radial segregation of particles on top surface, diffusion guides particle segregation across the sample thickness. Furthermore, isolated islands of nanotitania (~100-500 nm) were found embedded in a matrix of silica due to hetero-aggregation caused by silica-titania interaction in the centre of the droplet. The first phenomenon which shows dependency on the deployment order of nanoparticles has been explained in Part A of the discussion section. Titania clustering in silica matrix is found to be invariant to the aforementioned deployment order and is discussed briefly in Part B. Presented work demonstrates the simplicity of the droplet deployment methodology in producing controlled multicomponent and multilayered surfaces while utilizing the naturally occurring capillary flow induced particle transport. Additionally, particle clustering reported here could form the proof of concept in assembling nanoparticles of different compositions into complex geometrical patterns over a wide range of length scales.

*Corresponding author: Tel: +91 080 2293 3367
Email: sbasu@mecheng.iisc.ernet.in (S. Basu)

Experimental Details

Material preparation

The experimental studies reported here used aqueous dispersions of colloidal nanosilica (Ludox® TM40 with a mean particle diameter of 20-22 nm and particle concentration of 40 wt.% (weight percentage) from Sigma Aldrich) and colloidal nanotitania (Anatase phase, HNO_3 stabilized with a mean particle diameter of 4-8 nm and particle concentration of 20 wt.% from Reinste Nanoventure). Both were diluted to 4 wt. % with de-ionized water. To maintain stability of the diluted dispersions and thus prevent pre-mature particle sedimentation both nanosilica and nanotitania were subjected to sonication for 30 minutes and 60 minutes respectively. After sonication the respective zeta potential values (using Henry's formula) for both silica and titania dispersions were measured using ZetaPALS (Brookhaven's USA). The average zeta potential for titania sol (of pH 1.12) was found to be 49.1 $\pm$ 7mV and the same for silica sol (of pH 9.73) was -58.6 $\pm$ 3.89mV.

Experimental Setup

The setup consists of a microscope glass slide (Superfrost® Plus, Fisherbrand) housed inside a transparent acrylic chamber (10.5x10.5x3 cm^3) to nullify any external convection effect. Fresh slides are used for each experimental run. Required volume (3 +/-0.015 µl) of liquid sample is dispensed using a syringe pump (New Era Pump Systems, Inc, USA) for improved accuracy. A slit made on the chamber wall allows the syringe to be positioned on top of the glass slide for droplet deployment. Post-deployment, the drying droplet is imaged from top and side using CCD cameras (NR3-S1 & Motionscope M5, IDT cameras) coupled with zoom lens assemblies (1X magnification; Navitar lens). Both the cameras have been synchronized using a pulse generator (BNC 575) to acquire images every 10 seconds. LED and Halogen light (Schott LLS and ThorLabs respectively) sources have been used for illuminating the droplet for imaging purpose.

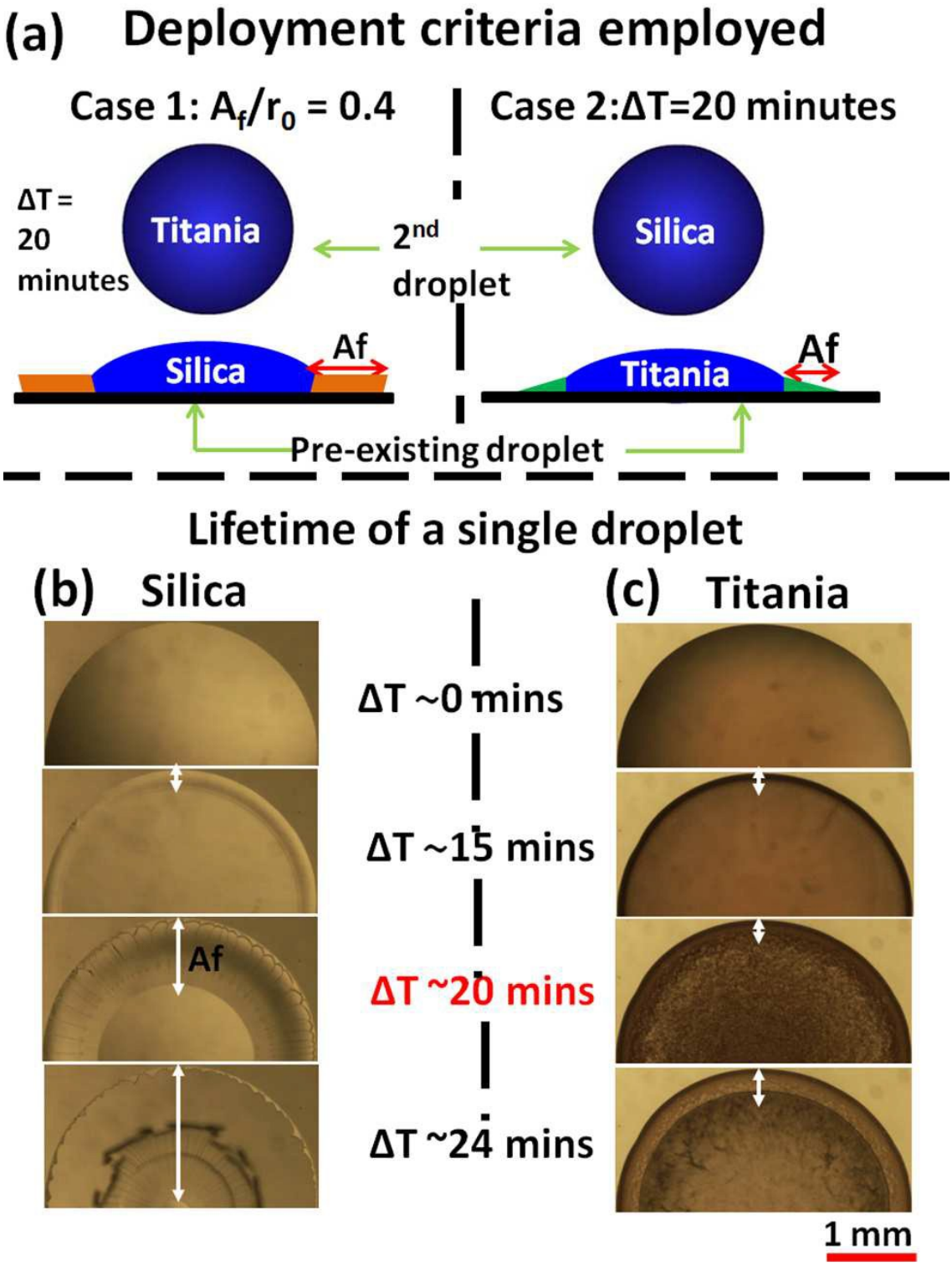

Fig. 1 : (a) schematic showing droplet deployment strategy case 1 (A_f/r_0=0.4) and for case 2 (ΔT=20 minutes) where A_f=agglomeration front , r_0=initial contact radius of first droplet, ΔT=time delay between deployment of two droplets (b) single nanosilica droplet (4wt. %): Af (marked by white

arrows) grows and extends till the centre (Af/r0=1)(c) Single nanotitania droplet (4 wt.%): Af arrested (Af/r0=0.2) and resembles a band like structure throughout the droplet lifetime.

Experimental Procedure

The initial contact angle of both single nanosilica and nanotitania droplet on glass was measured using contact angle meter (HO-IAD-CAM-01A, Holmarc, India) and found to be between 35°-40° (based on 6 experimental runs). Two sets of experiments were conducted (referred to as case 1 and case 2) using different droplet deployment strategies as shown in Fig. 1a. The strategies employed are based on different behaviour of individual silica and titania droplets drying on glass governed by DLVO force between particle and substrate [27]. Fig. 1b shows snapshots of the drying process at different time instants corresponding to a single nanosilica droplet. It is seen that due to the higher pH of silica sol (~9), the nature of DLVO force between the silica particles and the substrate is repulsive. This repulsion and outward capillary flow leads to substantial transport of particles towards the pinned outer periphery without adhering to the substrate at intermediate radial locations. With continuous evaporation, the particles agglomerate at the edge and the agglomeration front grows radially inwards as shown in Fig. 1b. As evaporation progresses, the agglomeration front shows a radially inward growth and finally extends till the centre [26]. In case 1 [Fig. 1a], nanosilica droplet of 4 wt. % by concentration is initially dispensed on glass slide and allowed to naturally evaporate. As soon as the agglomeration front reaches 40% of the initial contact radius, nanotitania droplet of same volume and concentration is dispensed co-axially on top of the partially dried precipitate.

Fig. 1c shows the progressive changes in morphology of a single nanotitania droplet. For titania sol, a lower pH (~1) results in attractive DLVO force between titania particles and the substrate. This lead to uniform and thicker deposits (particles adhering to the substrate) near the droplet center. However a thick outer ring like deposit (as shown in Fig. 1c) is still significant primarily due to the outward capillary flow (pinned contact line). The mechanism for this sort of uniform deposit has already been explained by Bhardwaj et al [27]. As opposed to the continuous growth of agglomeration front extending to the center, nanotitania exhibits an arrested solid front that does not extend beyond 20 % of the initial radius [Fig. 1b]. Thus in case 2 when nanotitania droplet is dispensed first, its solid front

growth can no longer be used as an indicator for dispensing the second droplet (nanosilica in this case). In such a scenario, the average time delay (ΔT=20 mins) between the dispensing of two droplets in case 1 (when nanosilica agglomeration front is 40% of initial contact radius) was noted and subsequently used for deployment of second droplet (nanosilica) in case 2 (see Fig. 1a). The dried out samples were preserved for optical microscopy and other characterization techniques.

Characterization

Optical Characterization

Bright field microscopy was performed on the preserved precipitates using an upright metallurgical microscope (NJF-120A) with 4x/0.1 planar objective. Snapshots of the samples were acquired at 2048 x 1528 pixels (pixel size = 2.5 x 2.5 µm) using a CMOS camera (Discovery CH 30).

Energy Dispersive X-ray Analysis (EDXA)

Energy Dispersive X-ray Analysis (EDXA) was done using Ultra 55 FE-SEM coupled with an EDX system (Oxford Instruments). Samples were gold sputtered (150 nm thickness) using Q150R ES (Quorum Technologies, UK). Acceleration voltage was kept at 15 kV and working distance was varied based on the method of scan as discussed below. EDX data was corrected using INCA software (Oxford Instruments). SiO_2 was used for the calibration of the analyzer.

In this paper, we performed EDXA using specific interrogation windows to calculate the elemental weight variation and then combined them using atomic balance to obtain the relative weight percentage of silica with respect to titania in that particular region. Such interrogation windows spanning the radial as well as the vertical cross section of the final precipitate give an idea of the compositional variation across the dry precipitate. In the following discussion, any reference to particle concentration would imply the relative value of silica with respect to titania in a given interrogation window.

Three scan methods were employed. Method 1 involved scanning across the top surface of the preserved sample. A working distance of 15 mm was maintained. Window size for each scan was kept constant at 12 µm x 12 µm.

Method 2 involved cleaving the preserved sample along its diameter to expose the cross section. Subsequently the sample was mounted vertically with respect to the EDX electron gun. At discrete radial locations ranging from the edge to the centre of the precipitate, EDXA was performed along the cross-sectional depth of the sample. Working distance was fixed at 15 mm with window size of 2.6 µm x 2.6 µm for edge scans. Working distance of 11 mm and window size of 82 nm x 82 nm was used for the centre region. Method 3 involved imaging of small scale structures observed at high magnifications in the central region of the precipitate. Working distance of 15 mm and window size of 270 x 270 nm was used.

Results and discussions

The present work reports a novel stacking mechanism (double droplet) that can tailor morphological and compositional variations in a naturally dried bi-component droplet based on in-situ mixing and order of deployment of individual components. As mentioned earlier, nanosilica droplet followed by nanotitania is referred to as case 1 while the reverse deployment order is referred to as case 2.

Part A: Observations on Macroscale Segregation

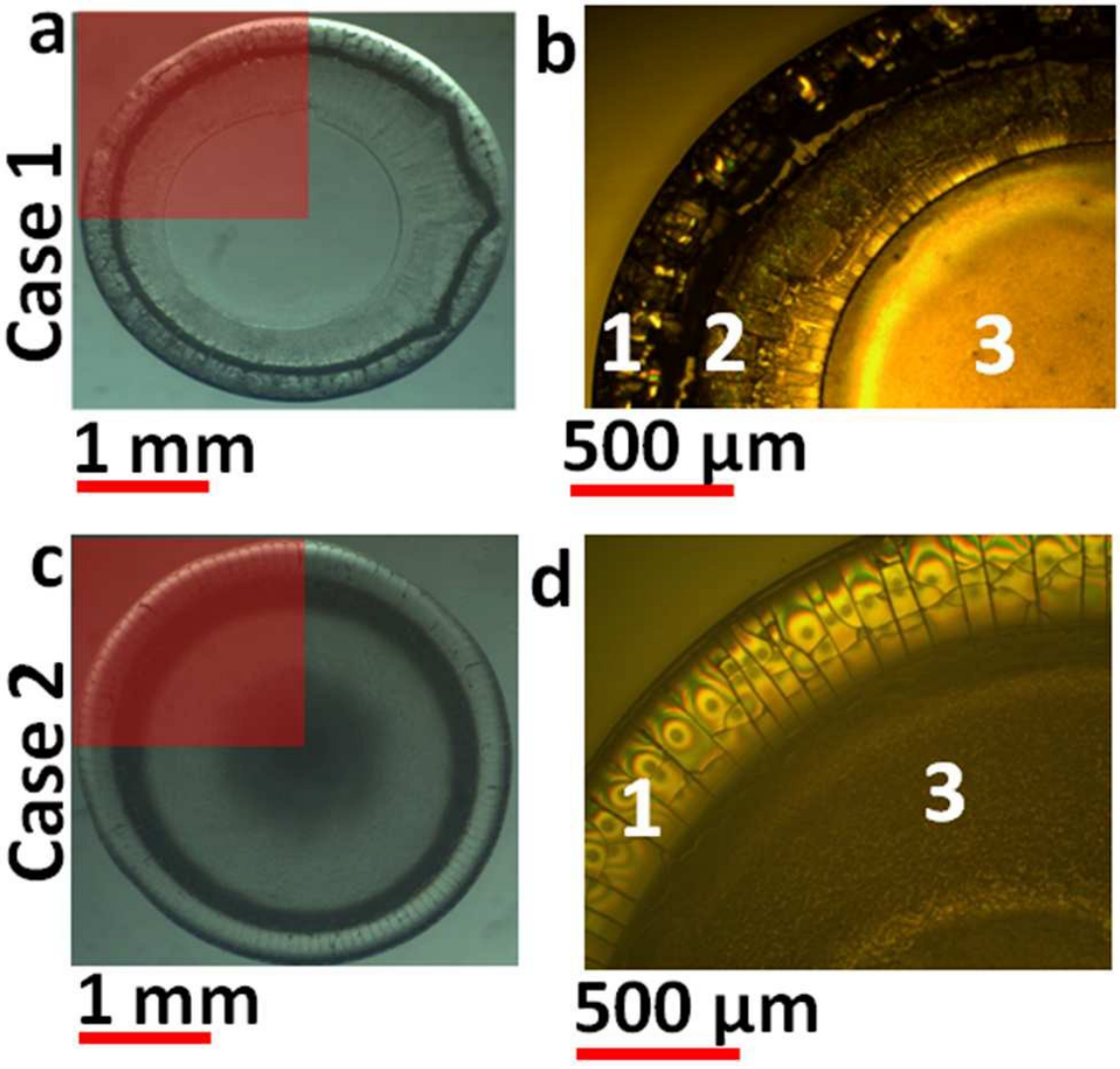

Figure 2: Final precipitate of nanosilica-nanotitania droplet (a) Case 1:nanotitania deployed on nanosilica (b) magnified view showing three distinct zones (1,2 and 3) (c) Case 2: nanosilica deployed on nanotitania (d) magnified view showing two distinct zones (1 and 3)

Figure 2 shows snapshots of dried out double droplet corresponding to cases 1 and 2 [Figs. 1a and 1c]. Portion of the precipitate [Fig. 2a; case 1] when magnified under a microscope

reveals three distinct zones. Based on the intensity variation of the presented image, it is claimed that the sample thickness has a gradually tapering profile from edge to centre as corroborated by SEM images reported later. The thicker and darker outer periphery is labelled zone 1 while the innermost, almost crack free region is marked as zone 3. The annular region with intermediate thickness is denoted as zone 2. Case 2 depicted in Figs. 2c and 2d has similar radially varying pattern except for the absence of zone 2.

Based on the morphological variations observed and the bi-component nature of the deposit, it was necessary to quantify the compositional variations across the surface as well as the depth of the precipitate using EDXA. The top surface composition was obtained using method 1 while the depth variation was characterized by method 2.

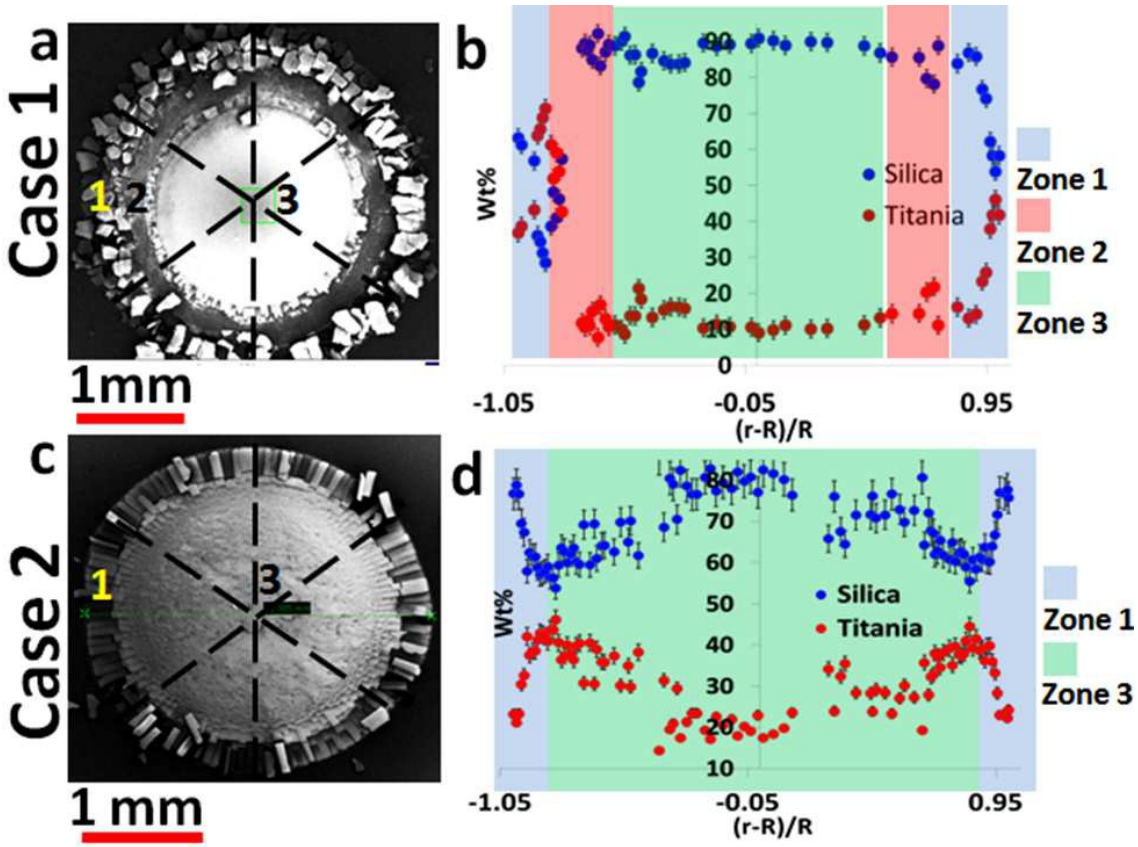

Figure 3: EDXA results showing the radial variation in composition across the top surface of the droplet deposit. (a) SEM of case 1 showing zones 1 (blue), 2(red) and 3(green) labelled. Dashed lines show EDXA scan path (b) plot of compositional variation (Wt%) of nanosilica (red markers) and nanotitania (blue markers) across the normalized radius of the final precipitate where r is any location on the top surface of precipitate and R is the final radius of the precipitate (c) SEM

snapshot of case 2 with zones 1(blue) and 3(green) labelled (d) compositional plot for nanosilica and nanotitania in case 2 where the notations are same as case 1.

Fig. 3a shows the preserved sample (for case 1) used for EDXA. Dotted lines show the scan paths used. Fig. 3b shows compositional variation across the radial span of the precipitate. Concentration of nanosilica (~60 wt. %) is higher than nanotitania (~40 wt. %) in the outermost region of zone 1. Both the components displayed non-monotonic trends within zone 1 [Fig. 3b]. In zone 2, both nanosilica and nanotitania concentrations reach peak values (~90 wt. % vs. 10 wt. % respectively). This level is maintained throughout zones 2 and 3.

In Case 2 (Fig. 3c), compositional variation [Fig. 3d] shows nanosilica concentration to be higher than nanotitania at the outermost edge of zone 1 and starts decreasing towards the centre of the deposit. However, the change in concentration of silica is non-monotonic and starts to increase from the edge of zone 1 (titania again shows the reverse trend).

In zone 3, concentration of nanotitania decreases and reaches a minimum at the center of the precipitate while nanosilica concentration increases to a peak value at the same location. When compared to Case 1, concentration of nanosilica is much higher than nanotitania along the top surface of the deposit (for all radial scans). From both the cases presented, we can conclude that, irrespective of the material deployment order, concentration of nanosilica is always higher than nanotitania in zone 3 compared to zone 1.

The next line of analysis probes into the composition variation across the depth of the deposit. EDXA was performed using method 2. In the following discussion, zone 1 has been sub divided into zone 1a and zone 1b.

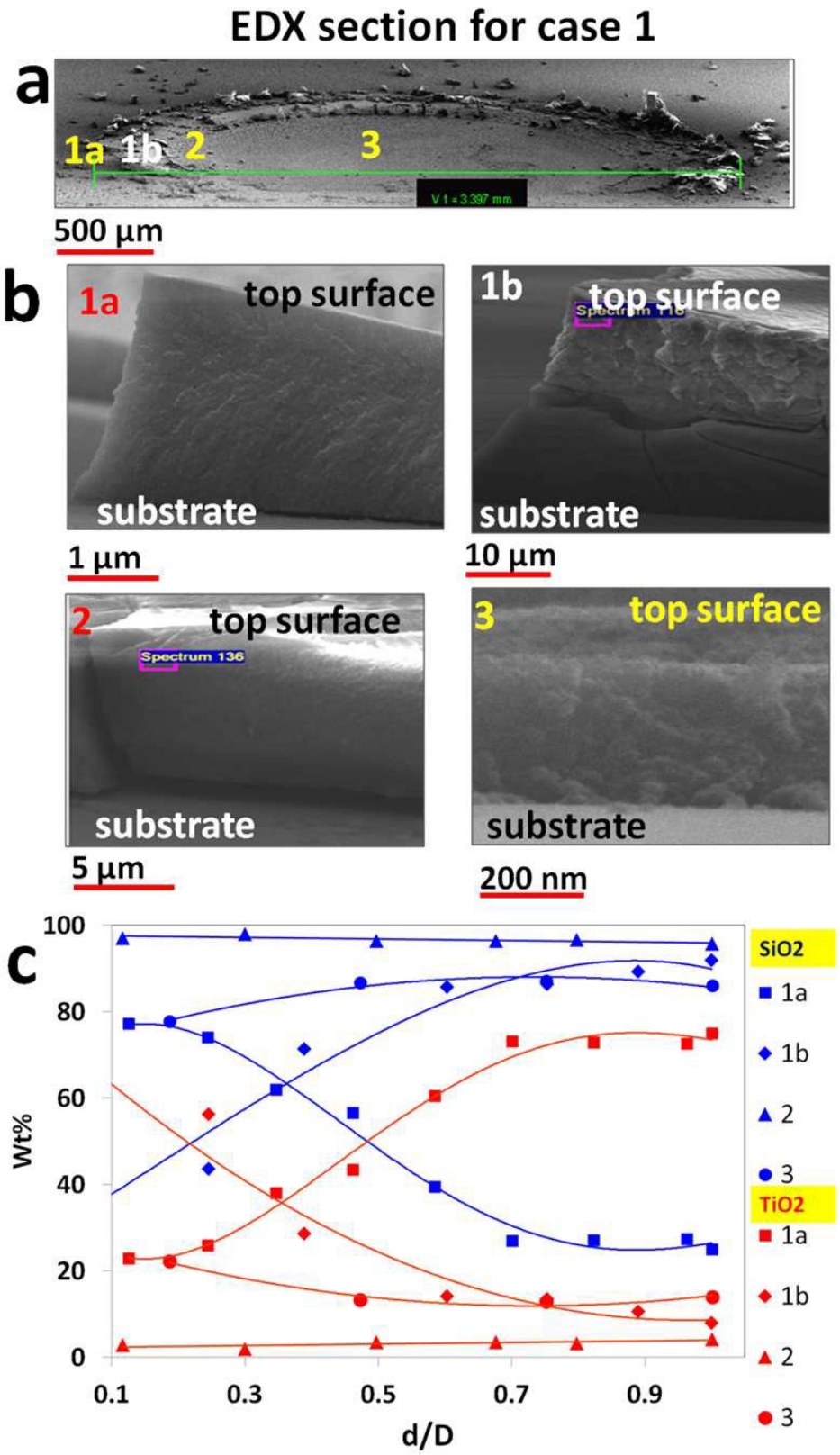

Figure 4: EDXA results showing the variation of composition of silica (blue) and titania (red) across the depth (a) discrete locations across the cleaved sample of case 1 used for depth EDXA also showing thickness profile (b) magnified images showing scanned regions in zones 1a, 1b, 2 and 3 (c) plot showing compositional variation (Wt. %) across vertical cross-section of sample where d is any depth below the top surface and D is the thickness of the precipitate where EDXA was done.

Figures 4a shows the diameter along which the samples were cleaved for EDXA scans in case 1. In Fig. 4b, snapshots of regions, where EDXA was done, are provided to show the thickness variation of the final precipitate from zone 1 to zone 3. It is observed that the average thickness of the precipitate is 5-7 µm in zone 1a, which increases to a peak value of 25-30 µm in zone 1b. Beyond 1b, it starts to taper down, decreasing to 10-12 µm in zone 2 and 400 nm-800 nm in zone 3. Fig. 4c shows the compositional variation across the cross section of the precipitate at the discrete locations shown in Fig. 4b. In zone 1a, silica decreases from 80 wt.% to 20 wt.% while titania increases from 20 wt.% to 80 wt.% along the depth from top surface. In zone 1b the trend reverses. Silica increases from 40 wt.% to 95 wt.% while titania decreases from 60 wt.% to 5 wt.%. Zone 2 shows almost no presence of titania (< 5 wt. %) compared to silica (>95 wt. %). In zone 3, silica concentration decreases to ~80 wt. % while concentration of titania increases to ~20 wt. %. For both zones 2 and 3, the respective concentrations of silica and titania remain constant with depth from the top surface.

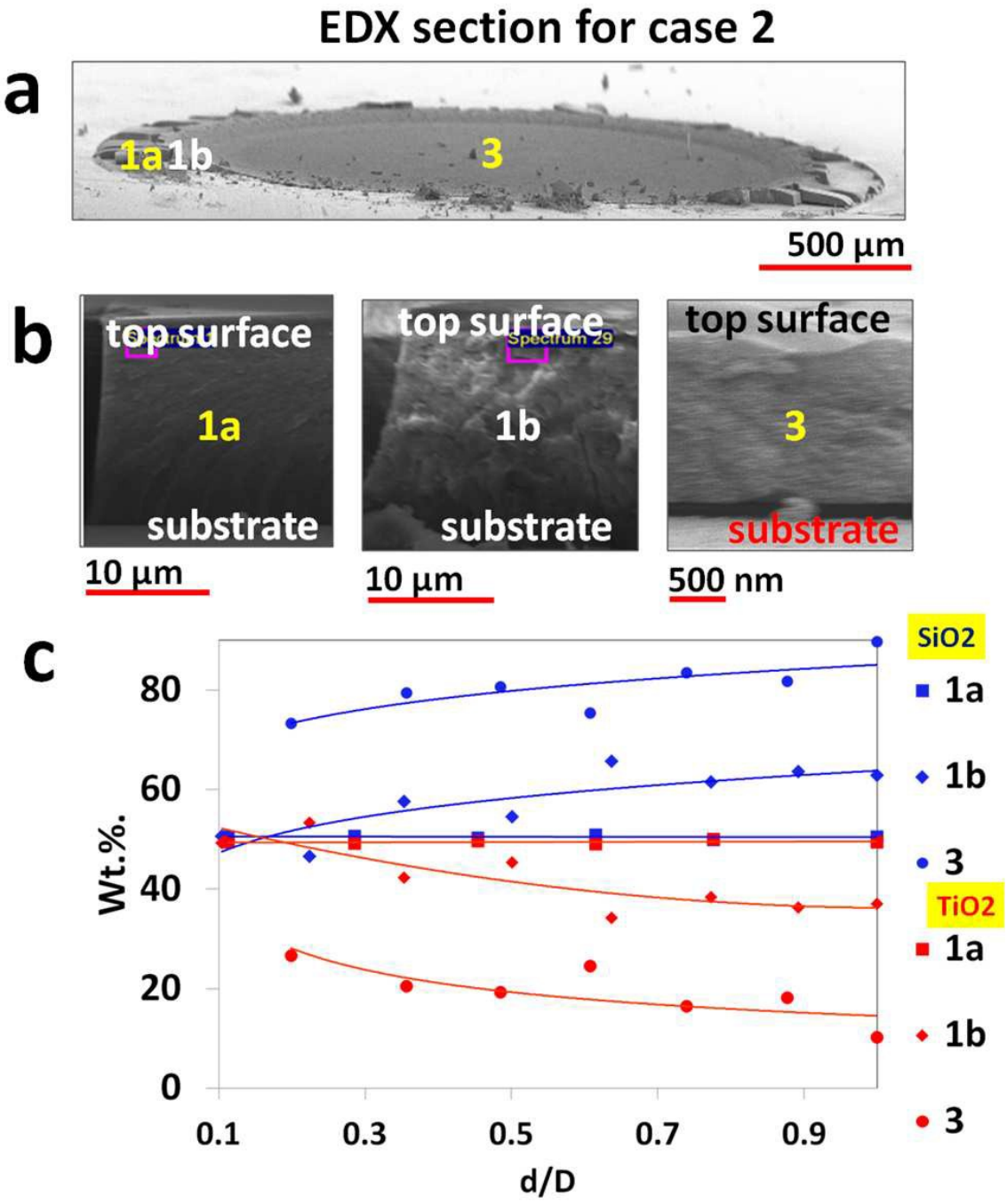

Figure 5: EDXA results showing the variation of composition across the depth (a) discrete locations across the cleaved sample of case 2 used for depth EDXA also showing thickness profile (b) magnified images showing scanned regions in zones 1a, 1b and 3 (c) plot showing compositional variation (Wt. %) across vertical cross-section of sample where d is any depth below the top surface and D is the thickness of the precipitate where EDXA was done.

For case 2 as depicted in Fig. 5, another interesting observation unfolds. The thickness profile [Fig. 5b] is different from the one seen in case 1. Zone 1a has a thickness of 20-25 µm (5-7 µm in case 1) which increases to 24-30 µm in zone 1b (almost equal to case 1). In zone 3, deposit thickness is about 2-3 µm (400- 800 nm in case 1). Compositional make up as shown in Fig. 4c displays equi-proportional presence of silica-titania concentration in zone 1a. In zone 1b, the plot shows a slight divergence as silica concentration increases with depth (50-60 wt. %) while titania concentration shows a slight dip (50-40 wt.%). In zone 3, concentration of nanosilica (75-85 wt. %) is higher than nanotitania (25-15 wt.%) at any depth from the top surface. Comparing cases 1 and 2, we make two notable observations. First, nanosilica and nanotitania concentrations in zones 1a and 1b of case 2 are similar (unlike case 1). Second, the variation in sample thickness from edge (zone 1) to centre (zone 3) in case 1 is much higher (~30 µm to ~600 nm) than in case 2 (30 µm to ~2 µm).

We observe that for a given (r, h) location, the composition remains same for all Θ (azimuthal symmetry of composition; Fig. 3). This allows us to compute the volume fraction of silica and titania at any elemental volume of the precipitate as shown in Fig. 6a. We have used additional information that the void fraction in any elemental volume is ~ 0.4 as seen in the SEM images (inset Fig 6a; random closed packing).

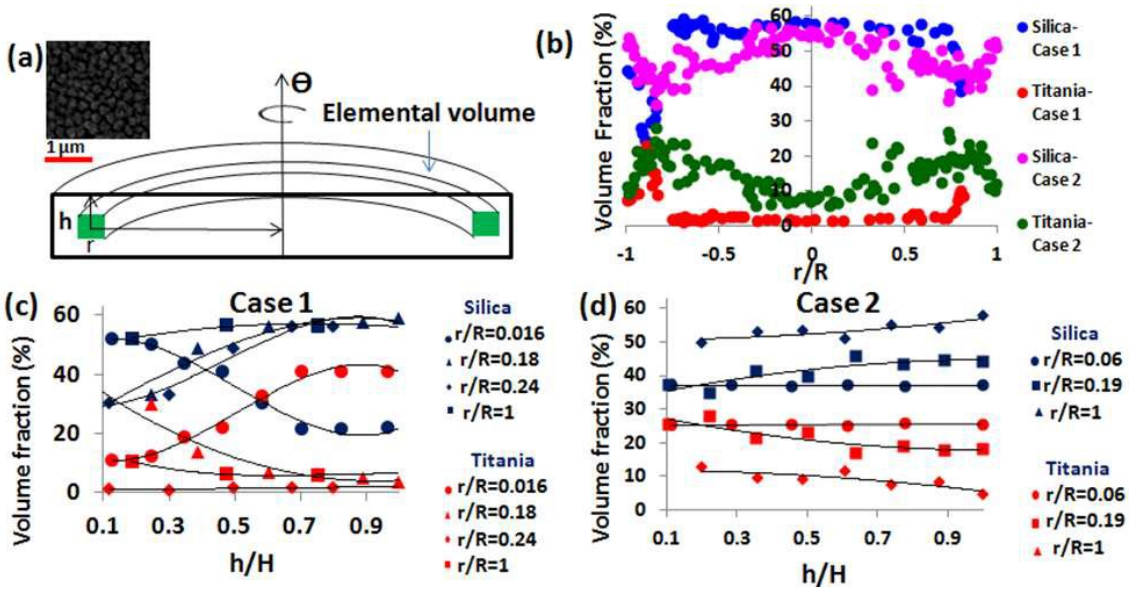

Figure 6: Summary of volume fraction data obtained from weight percentage data (a) Cross-sectional view of final deposit. Green squares represent EDAX scan windows (~ 10 µm at edge to ~

80 nm at centre). Elemental volume exhibits an azimuthally (Θ) symmetrical composition. EDAX has been performed at different (r, h, Θ) locations across the deposit structure. (Inset) SEM showing silica particle packing. Void fraction is ~ 0.4 (randomly closed packing). (b) Variation in volume fraction of silica and titania shown as a function of depth (h) for various radial (r) locations. Here H is the thickness of the deposit at a given radial location (r) of the deposit. (d) same plot as (c) for case 2.

The calculated the volume fraction is presented in Fig. 6b (volume percentage variation in radial directions as in cases 1 and 2), Fig. 6c and 6d (volume percentage variation in the cross-section depth wise direction as in cases 1 and 2 respectively). The plots in Fig. 6(b-d) show similar trends as those shown in the corresponding plots of Figs. 3-5.

Part A: Discussions on macroscale segregation

This section attempts to explain the phenomenon described in the previous section. Two issues are being addressed here. First involves nature of the final double droplet precipitate in terms of radial composition (Fig. 3) and its dependence on deployment order of droplets. The second issue involves the variation in composition along the thickness of the sample (Fig. 4 and Fig. 5) and its dependence on deployment order of the droplets.

Before we proceed any further on double droplet evaporation phenomenon, it is worth recalling a few salient points on single, sessile droplet evaporation from literature. A single sessile droplet on a smooth, non-absorbing surface with contact angle value of less than 90° follows Constant Contact Radius (CCR) mode of evaporation [17]. Here the contact line remains pinned to the substrate while evaporation results in contact angle reduction. Towards the very end of its drying state, the contact line gets de-pinned and starts receding inwards till the entire droplet evaporates. For particle laden droplet, solvent loss at the edge is replenished from centre resulting in bulk transport of particles forming a coffee-ring like pattern [15]. In the current discussion, no attempt is made towards explaining the droplet evaporation paradox as reported by Zhao [28].

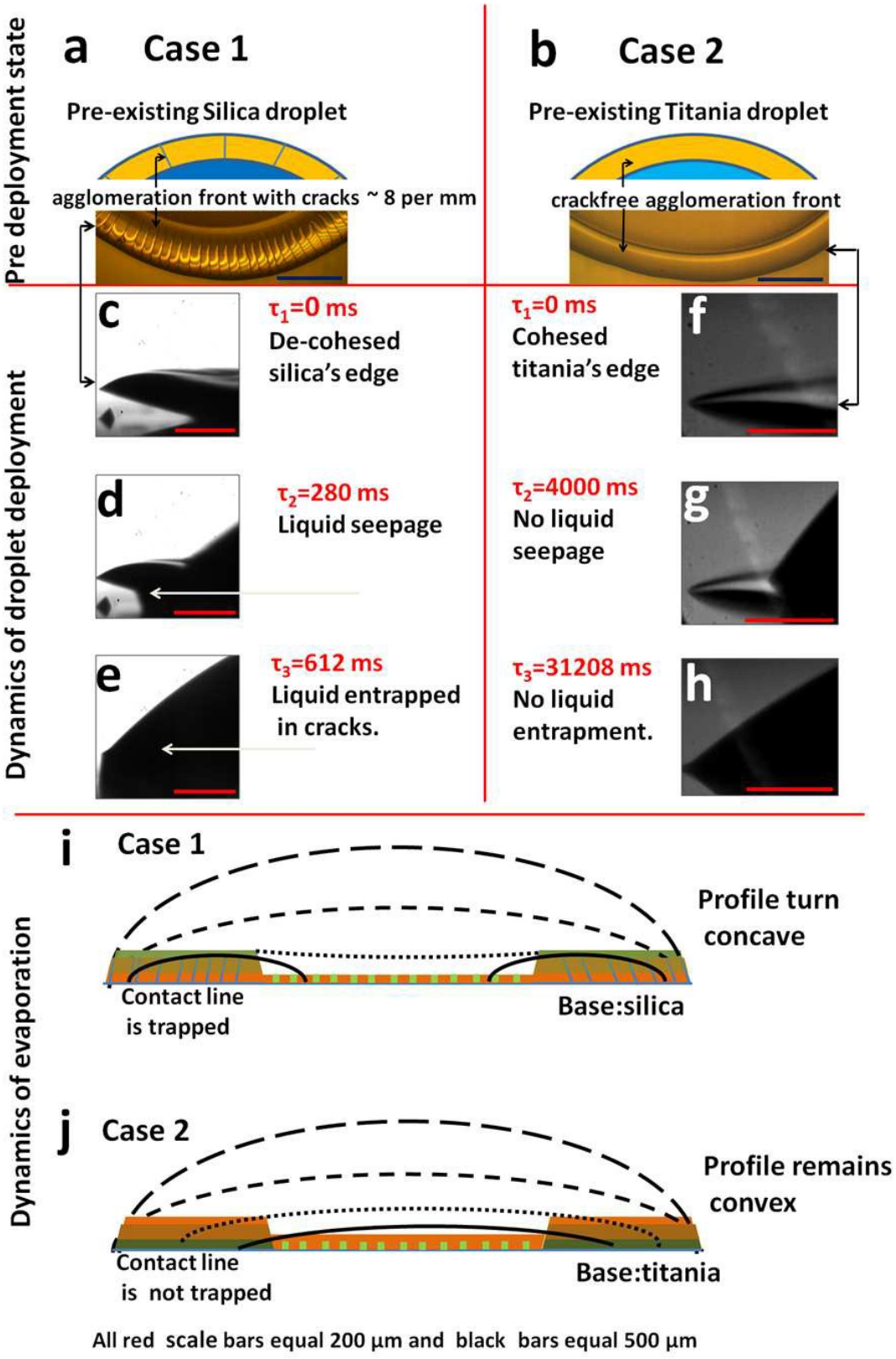

All red scale bars equal 200 µm and black bars equal 500 µm

Figure 7: (a) cracks in agglomeration front of a pre-existing nanosilica droplet just before nanotitania is deployed; an average of 8 cracks per mm of the circumference (b) crack free agglomeration front of a pre-existing nanotitania droplet just before nanosilica is deployed;0 cracks per mm (c) τ_1=0 ms pre-deployment of 2nd droplet:de-pinned edge of nanosilica (d) τ_2=280 ms post deployment: seepage of nanotitania through nanosilica's cracked solid edge (e) τ_3=612 ms post deployment: consequent entrapment of nanotitania's contact line within the cracks of nanosilica (f) τ_1=0 ms pre-deployment of 2nd droplet: Pinned edge of nanotitania (g) τ_2=4000 ms post deployment: deployed nanosilica appears to flow over nanotitania's solid edge (h) τ_3=31208 ms post deployment: nanosilica has engulfed nanotitania where τ is the time instant post deployment of the second droplet when the snapshot was acquired (i) schematic of case 1 drying process: dotted line shows pinned contact edge and gradually flattening curvature of droplet with evaporation. Nanotitania (green) is shown to accumulate over nanosilica (brown). Green squares in centre represent precipitates of nanotitania embedded into nanosilica (j) Schematic of case 2 drying process: dotted lines show the temporal progression of droplet profile. Contact line de-pins towards the end of drying process. Nanosilica (brown) accumulates over nanotitania (green). Lower number of pinning locations than case 1 due to the absence of cracks on the pre-existing agglomeration front.

In case 1 where nanosilica acts as the base droplet, Fig. 7(a) shows pre-existing droplet deposit edge with radial cracks in the agglomeration front. On the contrary, pre-existing nanotitania (Fig. 7(b)) droplet shows a crack free agglomeration front. Figs. 7(c-e) show the dynamic stages during droplet deployment in case 1. In addition to the occurrence of periodic cracks [Fig. 7a] on the solid edge of the pre-existing nanosilica droplet, it also appears to have de-pinned vertically from the native substrate [Fig. 7c]. When nanotitania is deployed upon this deposit, it seeps through the cracks of the pre-existing agglomeration front and wets the native substrate as seen after 280 ms of deploying the second droplet [Fig. 7d]. This results in entrapment of a small portion of nanotitania puddle within and beneath the cracked solid edge of nanosilica precipitate. In Fig. 7e, after ~ 600 ms of its deployment, titania has completely seeped through the silica precipitate.

In case 2, Fig. 7f shows the solid edge of pre-existing titania droplet to be pinned to the substrate prior to silica deployment. Fig. 7g shows that even after 4000 ms of its deployment, liquid from the silica droplet has not seeped through the titania precipitate since it is devoid of cracks. Hence no entrapment of nanosilica puddle happens in case 2. It

is worth noting that in case 1, liquid from the second droplet requires about 612 ms to seep through the entire pre-existing front while even after 31208 ms in case 2 no seepage or wetting of glass surface is evident. For both cases 1 and 2, the initial mode of evaporation remains similar to each other and resembles that of a single droplet. In case 1, a major portion of nanotitania is now trapped underneath the cracked deposit uniformly along the circumference. Multiple cracks further ensure stronger pinning of the liquid contact line and hence enhance particle transport (of the second droplet) towards the edge. Thus majority of nanotitania gets deposited at the periphery in zone 1 as can be seen from the thick edge in Fig. 2b. This also explains the higher concentration of titania in zone 1 and dominance of silica concentration in zone 2 and 3 [Fig. 3b]. Due to the absence of cracks in case 2 [Fig. 7b], pinning action is weaker and hence migration of silica particles towards the edge is diminished. Thus nanosilica concentration is higher at the centre in zone 3 and dwindles towards the edge in zone 1 [Fig. 3d]. Next the depth-wise compositional profile is explained.

As stated earlier, post deployment, a small volume of nanotitania seeps through nanosilica edge structure [Figs. 7c-e] and subsequently dries out. Thus zone 1a in case 1 [Fig. 4c] shows higher nanotitania concentration in layers nearer to the substrate while higher nanosilica concentration is observed at the upper layers (close to the top surface). As shown in Fig. 7(i), nanotitania (green colour) migrates towards edge and accumulates on the top layer of zone 1b. A small part of it diffuses into the pre-existing partially dried nanosilica layer (brown colour). Thus, nanotitania concentration is observed to be higher near the top surface in zone 1b [Fig. 4c]. Extra thickness at zone 1b as compared to zone 3 [Fig. 4b] may also be attributed to the enhanced transport of nanotitania from centre to the edge aided by the superior pinning action of the cracks in nanosilica. Since majority of deployed titania has migrated towards the edge, silica concentration dominates across all depths in zones 2 and 3.

In case 2, the pre-existing solid front of nanotitania on which nanosilica is deployed is almost crack free and does not allow any liquid seepage through it. Absence of cracks also results in weaker pinning of nanosilica's contact line and hence diminished transport of nanosilica towards edge. Hence almost equi-proportional presence of nanosilica and nanotitania in zone 1a (case 2) is seen in Fig. 5c. At this juncture of our analysis, we claim that the solid structure of nanotitania is more permeable to liquid as compared to the solid structure of

nanosilica allowing greater diffusion of deployed nanosilica into existing nanotitania structure. Also due to the lower edge-ward migration tendency of nanosilica, the thickness variation from zone 1 to 3 is also less drastic as compared to case 1.

Thus we propose that the deployment order is a very important parameter in the droplet based stacking of materials and may be used in controlled preparation of multi-component structures on functional surfaces for any variety of applications ranging from lab on a chip to surface patterning.

Part B: Observation and discussion on particle clustering

As we reported in the last section, the centre of the dried out deposit displays some distinct small scale structures embedded into bulk matrix that remain invariant to the order of deployment.

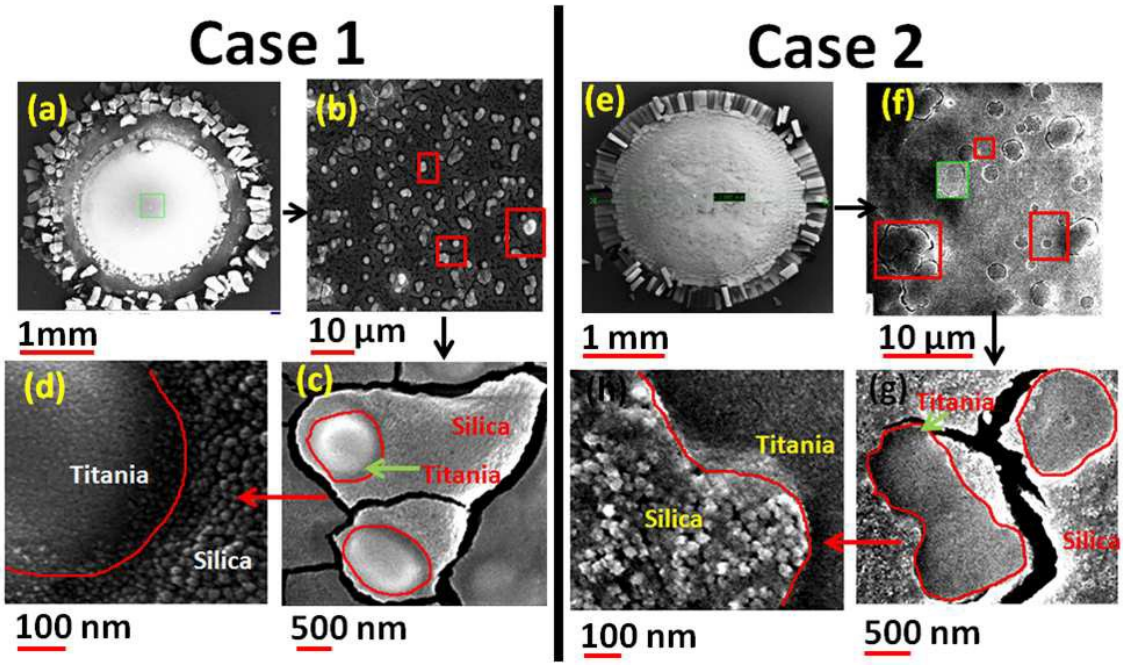

Fig 8: Embedded structures observed in the final precipitate (a) Case 1 preserved sample (b) zone 3 where the scattered islands (red boxes) of nanotitania are observed (c) magnified view of nanotitania surrounded by nanosilica (d) ultra magnified view showing larger nanosilica particles (20-22 nm) surrounding much smaller nanotitania particles (4-8 nm) (e-h) Case 2 follows the same order as (a-d).

Zone 3 in both cases 1 and 2 displays embedded microstructures as shown by the red boxes in Fig. 8b and Fig. 8f. Magnified snapshots of these regions (Fig. 8c for case 1 and Fig. 8g for case 2) show irregular shaped structures having an average size distribution of 100-500 nm. These micro-structures/clusters show higher nanotitania concentration (40 wt%) than the immediate neighbourhood. We conclude that these micro-clusters formed are predominantly titania in nature and invariant to the order of droplet deployment (since they

are observed in both cases 1 and 2). Magnified SEM images of the irregular shaped domains [Figs. 8c (case1) and 8g (case 2)] are presented in Figs 8d (case 1) and 8h (case 2). Smaller sized particles having an average size distribution of ~6 nm (nanotitania) are observed within the micro-structures/clusters surrounded by larger sized particles (of 20-22 nm silica). This is a conclusive proof of particle clustering observed in nanotitania when it interacts with nanosilica particles.

Individually both 4 wt. % dispersions of nanosilica and nanotitania were found to be stable as confirmed by their respective ζ-potential values reported in the material preparation section. But the opposite nature of these values makes them susceptible to aggregation. Thus, when a droplet of silica is mixed with a similar droplet of titania, scale like structures (measuring ~ 1.2 mm) were formed instantaneously. Since the second droplet is always deployed after a time delay, capillary flow would lead to edge deposition of particles. The magnitude of this delay determines the number of free particles present in the existing semi dry droplet which would be able to interact with the particles from the second droplet. Assuming all particles to be uniformly dispersed in the initial droplet, one can show that the number of free particles in the liquid pool as 5.875×10^{12}. To this, a 3 µl titania droplet containing 4.41×10^{13} particles is added.

A similar discussion could be made on silica deployed on titania droplet. However, to comment on the exact mechanism by which the titania forms micro-clusters and gets embedded in a matrix of silica particles requires rigorous investigations which is beyond the scope of the current work.

Conclusion

We presented a methodology which can be used with droplet based colloidal systems to obtain micro-patterned multi-component stack on a glass substrate. Experiments involved times delayed dispense of pure nanosilica and nanotitania droplets onto a glass slide in a coaxial manner. Two sets of experiments-one involving nanosilica dispensed upon nanotitania and the other involved nanotitania dispensed upon nanosilica-are reported here. Post evaporation, deposit patterns were both optically and compositionally characterized. Compositional variations were observed along the radial direction on the top

surface as well as the vertical depth of deposited stack. The state of the pre-existing solid edge (cracked or crack free) prior to the deployment of the second droplet and capillary flow determined the morphology as well as the compositional distribution of particles in the final precipitate. Since the second droplet was dispensed after a time delay on the first one, the pre-existing liquid pool and the deployed droplet underwent flocculation to produce clusters of particles at the centre. It was shown that irrespective of the order in which nanotitania and nanosilica were dispensed; nanotitania always formed the isolated clusters.

References

1. Nicolas Vogel, Surface Patterning with Colloidal Monolayers, Springer Theses (http://www.springer.com/series/8790), 2012.
2. O.D. Velev, A.M. Lenhoff and E.W. Kaler*, Science* 2000, 287,2240
3. K.E. Davis, W.B. Russel and W. J. Glantschnig, *Science* 1989, 245,507.
4. R.C. Salvarezza, L. Vazquez, H. Miguez, R. Mayoral, C. Lopez and F. Meseguer, *Phys. Rev. Lett.*1996, *77*, 4572.
5. M. Trau, D.A. Saville, I.A. Aksay, *Science* 1996, *272*, 706.
6. M. Holgado, F. Garcia-Santamaria, A. Blanco, M. Ibisate, A. Cintas, H. Miguez, C.J. Serna, C. Molpeceres, J. Requena, A. Mifsud, F. Meseguer, C. Lopez, *Langmuir* 1999, *15*, 4701.
7. P. Jiang, J. F. Bertone, K.S. Hwang and V.L. Colvin, *Chem. Mater.* 1999, 11, 2132.
8. Y. A. Vlasov, X.Z. Bo, J.C. Sturm and D.J. Norris, *Nature* 2001, 414, 289.
9. Y.H. Ye, F. LeBlanc, A. Hache and V.V. Truong, *Appl. Phys. Lett.* 2001, 78, 52.
10. Z.Z Gu, A. Fujishima and O. Sato, *Chem. Mater.* 2002, 14, 760.
11. A. Sanyal, S. Basu, S. Chowdhuri, P. Kabi and S. Chaudhuri, *Appl. Phy. Letts*. 2014, 104, 163108.
12. S.H. Park and Y.N. Xia, *Langmuir* 1999, 15, 266.
13. Patrick Wilhelm and Dietmar Stephan, *Journal of Photochemistry and Photobiology A: Chemistry* 2007, 185, 19.
14. Daniel M. Kuncicky and Orlin D. Velev, *Langmuir* 2008, 24, 1371.
15. E. Adachi, A.S. Dimitrov, K. Nagayama, *Langmuir* 1995, 11, 1057.
16. R. D. Deegan, O. Bakajin, T.F. Dupont, G. Huber, S.R. Nagel, T.A. Witten, *Nature* 1997, *389*, 827.
17. R. G. Picknett and R. J. Bexon, *Colloid Interface Sci.* 1977, 61, 336.

18. Vincent Dugas, Jerome Broutin, and Eliane Souteyrand, *Langmuir* 2005, 21, 9130.

19. Charles-Andre´ Fustin, Gunnar Glasser, Hans W. Spiess and Ulrich Jonas, *Langmuir* 2004, 20, 9114.

20. B.Y. Tay and M.J. Edirisinghe, *Proc. R. Soc. London, Ser. A* 2002, 458, 2039.

21. D.M. Kuncicky, K. Bose, K.D. Costa and O.D. Velev, *Chem. Mater*. 2007, 19, 141.

22. Yu.Yu. Tarasevich and D.M. Pravoslavnova, *Eur. Phys. J. E* 2011, 22, 311.

23. Mira T. Guo, Assaf Rotem, John A. Heyman and David A. Weitz, *Lab on a Chip* 2012, 12, 2146.

24. Dong-Ku Kang, M. Monsur Ali, Kaixiang Zhang, Susan S. Huang, Ellena Peterson, Michelle A. Digman, Enrico Gratton and Weian Zhao, *N. Comms.*2014, 5, 5427.

25. P. Kabi, S. Basu, A. Sanyal and S. Chaudhuri, *Appl. Phys. Lett ,* 2015, 063101, 106

26. A. Sanyal, S. Basu and S. Chaudhuri, *Chem. Engg. Science,* 2015, 123, 164.

27. Rajneesh Bhardwaj, Xiaohua Fang, Ponisseril Somasundaran and Daniel Attinger, *Langmuir* 2010*,* 26(11), 7833.

28. Yapu Zhao, *Theoretical & Applied Mechanics Letters* 2014, 4, 034002.

29. R. D. Deegan, O. Bakajin, T.F. Dupont, G. Huber, S.R. Nagel, T.A. Witten, *Phy. Rev. E.* 2000, 62, 756.